Optics Letters

Observation of whispering gallery modes through electron beam-induced deposition

F. J. Timmermans,[1,*] L. Chang,[1] H. A. G. M. van Wolferen,[2] A. T. M. Lenferink,[1] and C. Otto[1]

[1]Medical Cell BioPhysics Group, MIRA Institute, University of Twente, P.O. Box 217, 7500 AE Enschede, The Netherlands
[2]Transducers Science and Technology, MESA+ Institute, University of Twente, P.O. Box 217, 7500 AE Enschede, The Netherlands
*Corresponding author: f.j.timmermans@utwente.nl

Received 24 January 2017; revised 2 March 2017; accepted 3 March 2017; posted 3 March 2017 (Doc. ID 285288); published 27 March 2017

Surprisingly intense spectra of whispering gallery modes were observed in polymer microbeads after illumination with electrons in a scanning electron microscope and subsequent laser illumination and spectral analysis. It will be proposed that whispering gallery mode resonances became visible after local deposition of hydrocarbon material through electron beam-induced deposition. The illumination of deposited material with a near infrared laser generates a broad light spectrum, acting as a local "white light" source that couples, for favorable wavelengths, with the WGM sustained by the sphere. This facilitates a spectroscopic analysis of the WGM and provides the *Q*-factor and free spectral range for all investigated particles. The analysis by an integrated SEM and Raman micro-spectrometer offers a direct approach to the analysis of WGM resonators as they are, for instance, used in sensing.

OCIS codes: (300.0300) Spectroscopy; (230.5750) Resonators; (180.5655) Raman microscopy.

https://doi.org/10.1364/OL.42.001337

Optical microresonators confine light within a micro-cavity, which results in a significant increase of the energy density for resonator modes. In particular, whispering gallery modes (WGMs) are observed on microspheres that confine light propagating along the sphere surface by internal reflection. WGMs are employed as sensors for the detection of molecules or particles that attach on the sphere surface, where the change at the surface influences the WGM spectrum [1–7]. In other applications, the WGM has been used to achieve an increased light density, which enables Raman and spectroscopic analysis with a higher excitation energy density, thus achieving an enhanced signal [8,9]. Cavity-enhanced Raman spectroscopy has also been demonstrated for microscopic applications [10]. Optical ring resonators are furthermore applied for high-quality optical filters, in combination with coupled optical waveguides [3].

Polymer beads with diameters between 2 and 10 μm were used as microresonators. These beads are regularly used in Raman imaging as test samples due to their strong signals. It should be noted that no WGMs are observed from untreated polymer beads in normal Raman imaging. However, the detection of optical resonances during Raman analysis of microspheres has been used for morphology specific analysis; in those works, the WGM resonances are observed from a fluorescent component in the material [11–13].

We report on the use of an integrated optical microspectrometer in a scanning electron microscope (SEM) for analysis of WGM resonators. The optical microscope used in this project is a Raman microspectrometer with a 785 nm excitation laser. The optical objective is mounted inside the SEM vacuum chamber [14]. The electron beam is used to locally deposit hydro-carbon material that, upon laser illumination, acts as a white light source, with emission also in the near infrared [15,16]. Subsequent spectroscopic analysis reveals the WGM spectrum due to coupling of the excited white light emission with available modes. An analysis reveals the WGM spectrum, the mode free spectral range, *Q*-factors of observed modes, and relative mode intensities. Electron beam-induced deposition (EBID) is commonly used, for example, in fabrication of nanostructures [17,18], fabrication of electronic interconnects [17,19], and deposition of a carbon protective layer for TEM analysis [20]. Potential applications of integrated light and electron microscopy investigation of optical microresonators are non-destructive analysis methods for fabricated optical microresonators. This can be especially useful for waveguide structures prepared in combination with focused ion beam milling [21], as these are directly in-situ analyzed.

The integrated optical-electron microscope configuration enables fast analysis of WGM resonators on intermittent steps of SEM irradiation. The optical microscope laser is used to generate white light emission from the EBID of hydrocarbons; the subsequently excited WGMs are detected with the confocal spectrometer. The used samples are polystyrene beads with diameters ranging from 2 to 10 μm obtained from Polysciences, Inc.; the precise diameter specifications are reported, together with the results. WGM resonances are furthermore observed on 8 μm PMA and 6–13 μm glass beads, both obtained from Sigma-Aldrich. The beads are deposited on conducting metallic substrates designed to have a low light background and are suitable for correlative light and electron microscopy. The μrim™ substrates are obtained from BioTools, Inc. The treatment of the polymer beads is performed by irradiation with the SEM e-beam at a beam energy of 2 kV and a probe currents of 13–52 pA. Deposition of hydrocarbon material occurs mostly through

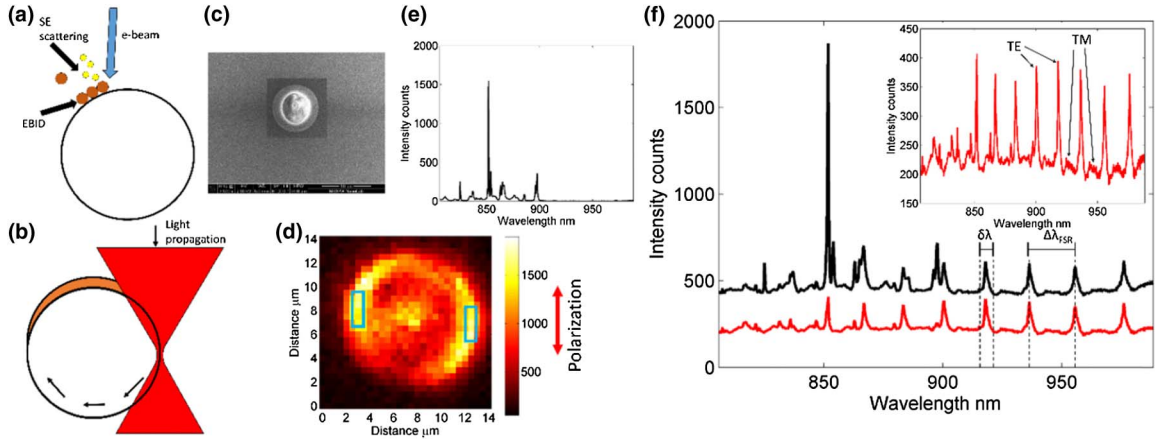

Fig. 1. Schematic representation of (a) the EBID process and (b) the incoupling of the excitation light into the WGM resonator. (c) SEM image showing the polymer bead; the effect of material deposition is noticeable as the dark square around the bead. (d) Optical intensity map showing the WGM signal intensity image. The laser polarization orientation is indicated with the red arrow. Two regions are indicated with blue squares; the spectra presented in (e) and (f) are obtained as the average from these pixels. (e) Polystyrene Raman spectrum observed for the untreated bead measured on the same region as the indicated positions in D. (f) Observation of whispering gallery modes, including the polystyrene Raman signal (black), with the polystyrene Raman signal subtracted (red). The inset shows the same red spectrum, enlarged to visualize both the TM and TE modes.

interaction of secondary electrons with trace gasses near the sample surface. This is because the lower energy of the SE electron, typically up to 50 eV, gives an increased interaction compared to the e-beam electrons [18,22]. The excitation of the WGM resonances is performed with 1–3 mW of 785 nm laser light, which is a sufficiently low irradiation to prevent bleaching or sample damage.

Spectra observed from the EBID hydrocarbon material show a high photoluminescence contribution over the full measured spectral range. The Raman band between 1400 and 1600 cm^{-1}, associated with amorphous carbon [23], is typically not observed in the investigation of the EBID treated resonator. In another work, Raman analysis of amorphous hydrocarbon material shows similar results with a fluorescence background observed for the EBID on an organic material (resin), and with the typical amorphous carbon Raman spectrum observed for the EBID on an inorganic (cinnabar) substrate [15,16]. The literature confirms that the EBID signal is substrate dependent, and that EBID provides a broadband spectrum, which is found to be suitable for coupling with the optical resonator modes.

EBID is performed on the top half of the bead, as indicated in Fig. 1(a). After the SEM treatment and incremental steps of the treatment process, a micro-spectroscopic analysis of the WGM spectrum is performed. The 785 nm laser excitation light is coupled into the sphere with a 0.65 NA optical objective. Due to the excitation direction light, propagation occurs along the vertical cross section of the bead, as schematically represented in Fig. 1(b). A SEM image of the treated polymer bead is shown in Fig. 1(c); the area on which EBID is performed is visible as a dark square. Furthermore, the charging effects are visible on the center of the bead as a white ring; the outer circumference of the bead does not undergo charging effects due to charge neutralization of higher SE scattering from the surface [24]. The full WGM resonator is scanned with the confocal spectrometer to spatially resolve the positions for excitation and detection of the WGMs. The optical image is shown in Fig. 1(d), showing the intensity in the counts of a single resonator band. Two regions are indicated in squares showing on which the positions the spectra are recorded for resonator analysis. The excitation laser light polarization is oriented along the y-axis as indicated in Fig. 1(d). In Fig. 1(e), the Raman spectrum from an untreated polystyrene bead is presented. The spectrum is obtained from the areas indicated in Fig. 1(d) and is identical to the standard Raman spectrum of polystyrene. We notice that no WGM resonator signal is observed for the untreated bead. Figure 1(f) shows the measured spectrum (black) after EBID. The Raman spectrum of polystyrene is accompanied by additional fringes with a typical spacing in agreement with what is expected from WGM resonances. The spectrum (red) of the WGM resonances in Fig. 1(f) is obtained after subtraction of the polystyrene Raman scattering spectrum. In the inset, the same red spectrum is repeated on an expanded amplitude scale to bring out fine details in the WGM response. Two resonator modes can be distinguished, indicated in the figure as the transverse electric (TE) and transverse magnetic (TM) mode. Assignment of the modes is based on $\lambda_{TM} < \lambda_{TE}$ and that the smaller peak is the TM mode [1,25]. The WGM spectrum is used to extract specifications from the resonator. The optical path length (OPL) of the resonator is defined with Eq. (1), where m and λ_m are the mode number and corresponding wavelength observed in the spectra, and $n_{g,\mathrm{eff}}$ is the effective group refractive index. The resonator quality factor (Q-factor) is determined from the width of the modes and the center frequency of the modes; see Eq. (2). A measurement of the Q-factor is limited to the resolution of the optical spectrometer, which is 5 cm^{-1}; this places an upper limit on the Q-factor magnitude of 2300. For the resonator presented in Fig. 1, the Q-factor varies between 350 and 650 for TE modes:

$$\mathrm{OPL} = 2\pi \cdot r \cdot n_{g,\mathrm{eff}} = m \cdot \lambda_m, \tag{1}$$

$$Q = \frac{\nu_0}{\delta\nu}. \tag{2}$$

It has been observed that the spatial dependence of the measured WGM signal follows approximately a cosine squared profile along the resonator circumference, as seen in Fig. 1(d). This profile originates from the laser excitation polarization, which has

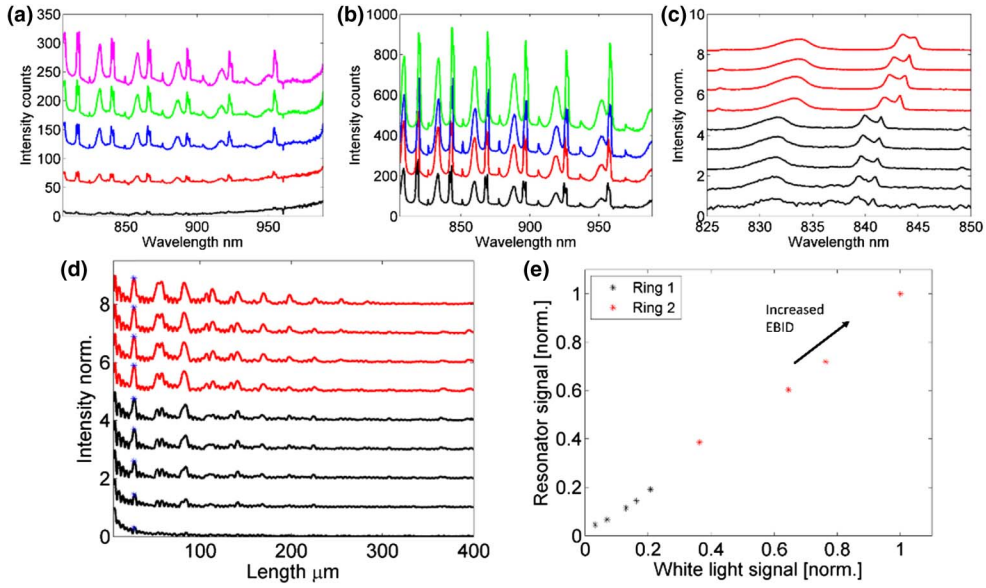

Fig. 2. (a) and (b) Observation of whispering gallery modes on two polystyrene beads, both 6 μm in diameter, with varying SEM irradiation steps. An offset between the consecutive spectra of (a) 50 counts is given for the first bead and (b) 100 counts for the second bead, with each consecutive step representing the spectrum measured after a new SEM EBID treatment. (c) Magnification of a single TM–TE mode combination of the spectra presented in (a) [black] and (b) [red]. Only a small change in the WGM spectra is observed for higher carbon deposition concentrations. The spectra are normalized to 1 and given an offset to improve a direct comparison of their shape. (d) FFT spectra of WGM resonances shown in (a) (black) and (b) (red). The optical path length of the resonators is identified from the first-order maximum 27.2 μm (e) ratio of the detected signal intensity of the WGM resonances versus the observed white light emission intensity from EBID material. The white light emission intensity is measured on the center of the treated polystyrene sphere as the smooth baseline under the Raman and WGM peaks. The direction of the increased EBID is indicated with an arrow.

been confirmed by varying the excitation light polarization for 0°, 45°, 90°, and 135° (data not shown). The measurements show that the observed resonator signal profile rotates with the laser polarization. It can be concluded that an optimized resonator signal is measured for light polarized along the bead surface, as is demonstrated in Fig. 1(d); an optimized signal is measured on this location indicated in with blue squares. It can be concluded that this provides an optimized propagation of the excitation light in the resonator through lower bending losses. This results in a higher excitation light density in the resonator, thus achieving an increased WGM signal.

An analysis of WGM resonators reveals an increasing resonance signal as a result of increased electron irradiation. This is demonstrated through incremental SEM irradiation steps with an intermediate spectroscopic analysis of the treated resonator. The results are presented in Fig. 2. Polystyrene beads of 6 μm in diameter were used for this experiment. Figure 2(a) shows the observed spectra after the irradiation of a polystyrene bead's top surface with a cumulative electron dose of $[14.6, 58.6, 132, 176, \text{and } 249]\ e^- \cdot nm^{-2}$; Fig. 2(b) shows spectra on a second polystyrene bead for an electron dose of $[310, 621, 932, \text{and } 1242]\ e^- \cdot nm^{-2}$; the spectra are vertically offset for clarity for Fig. 2(a) with incremental steps of 50 counts and for Fig. 2(b) with steps of 100 counts. The polystyrene Raman signal is subtracted from all the observed spectra to visualize only the WGM resonances. It is observed that the WGM Q-factor undergoes little change upon an increase of the irradiation dose. However, a shift of the WGM spectrum is observed; this shift is a result of a change in the refractive index of the surrounding medium caused by material deposition [6,26]. This is shown with more detail in Fig. 2(c), where a single TM and TE mode of the normalized spectra shown in Fig. 2(a) [black] and Fig. 2(b) [red] is presented. Figure 2(d) shows the fast Fourier transform (FFT) spectra of the WGM signals from Fig. 2(a) [black] and Fig. 2(b) [red]. The FFT spectra show clearly the optical path length of the resonance modes. The first-order resonance is found at the optical path length 27.2 μm, which corresponds to a 6 μm diameter ring and an effective group refractive index of 1.44, using Eq. (1). To determine the Q-factor, the free spectral ranges ($8.0 \times 10^2\ cm^{-1}$) and $\delta\nu$ ($30\ cm^{-1}$ for TE and $50\ cm^{-1}$ for TM) are obtained, which translates to a Q-factor up to 420 for TE modes and up to 235 for TM modes, with mode numbers 32 and 33. The resonator signal intensity increases close to linear with the increasing white light emission, which is linearly proportional to the laser power. Figure 2(e) presents the linear relationship between the resonator signal strength and the generated white light emission.

WGM resonances have also been observed in spheres of other materials. It is expected that most optically transparent spherical particles may sustain WGMs. Optical resonances were also observed in organic polymer poly(methyl acrylate) (PMA) and glass (SiO_2) beads after EBID treatment (data not shown).

Further analyses of polystyrene beads with different diameters reveal more properties of WGMs. Figures 3(a) and 3(b), respectively, show WGMs and their FFT spectra for polystyrene beads of 1.9, 3.05, 4.45, 6.0, and 10.2 μm in diameter. The diameters have been measured with SEM. The electron dose used for the analysis of the beads is, respectively, $[1.1, 1.0, 0.8, 1.2, 0.8] \times 10^3\ e^- \cdot nm^{-2}$. A significant increase in Q-factor for increasing resonator diameters is observed; the 3, 4.5, 6, and 10 μm diameter resonators have TE mode Q-factors up to 118, 163, 473, and 1155, respectively.

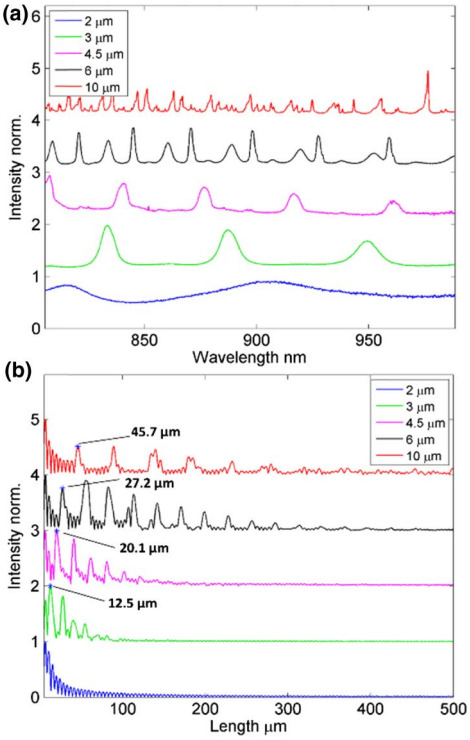

Fig. 3. (a) Observation of WGM resonances on polystyrene beads with diameters 2, 3, 4.5, 6, and 10 μm. (b) FFT of the spectra presented in (a). The optical path lengths of the resonators are indicated in the figure with the corresponding FFT bands.

The optical path length from the 3, 4.5, 6, and 10 μm beads is obtained from the first-order FFT peak: 12.5, 20.1, 27.2, and 45.7 μm, respectively, when dividing with the ring circumference of the effective group refractive index $n_{g,\mathrm{eff}}$ is obtained: 1.3, 1.44, 1.44, and 1.43. It is observed that an increasing diameter results in higher *Q*-factors, which is presumably due to smaller bending losses. The light frequency oscillations in the FFT spectra are due to window effects and are most prominent in the 0–20 μm length scale. The mode pattern for most of the beads is regular and can be interpreted in a straightforward manner, considering TE and TM mode propagation. Only for the largest investigated beads of 10 μm diameter higher-order modes and, therefore, more complicated resonator spectra, become visible, as presented in Fig. 3(a).

In summary, a surprising observation is reported of whispering gallery mode optical resonances after electron beam treatment of polymer micro-spheres. A proposed explanation for this observation originates from the EBID of material from the trace gasses in the vacuum chamber of a scanning electron microscope. The WGM resonances were observed in an optical spectroscopic analysis of the photoluminescence from EBID material after narrow-band laser illumination. The WGMs exist on the spheres before SEM treatment and are made visible by the EBID of hydrocarbon material. Broadband photoluminescence emission from EBID is excited with the Raman laser and couples to the local field of the WGM resonator and is observed with the optical spectrometer. Spectroscopic analysis with a Raman spectrometer integrated with the SEM provides direct access to the measurement of the free spectral range and *Q*-factors for modes observed in particles with different sizes and different materials. It has been observed that the resonator signal increases linearly with the electron dose which has been used to deposit hydrocarbon material. The photoluminescence spectral emission from deposited hydrocarbon material enables a direct observation of the resonator OPL after Fourier transformation of the luminescence spectra. Microscopic imaging of the resonator signal reveals areas of more efficient coupling of the local field to the WGM resonator versus areas with less efficient coupling. We conclude that an observed, surprising effect of intense WGM resonances in spheres with a combined SEM-Raman microscope is in full agreement with existing knowledge of cavity resonances. Thus, the combination of EBID and optical spectral analysis as a new method for analysis of WGM resonators has been presented and may provide opportunities for the characterization of WGM resonators for sensing applications and integrated optics.

Funding. Stichting voor de Technische Wetenschappen (STW) (12716).

REFERENCES

1. A. Francois and M. Himmelhaus, Sensors **9**, 6836 (2009).
2. J. Lutti, W. Langbein, and P. Borri, Appl. Phys. Lett. **93**, 151103 (2008).
3. A. B. Matsko, A. A. Savchenkov, D. Strekalov, V. S. Lichenko, and L. Maleki, IPN Prog. Rep. **42**, 1 (2005).
4. G. Farca, S. I. Shopova, and A. T. Rosenberger, Opt. Express **15**, 17443 (2007).
5. K. D. Heylman, N. Thakkar, E. H. Horak, S. C. Quillin, C. Cherqui, K. A. Knapper, D. J. Masiello, and R. H. Goldsmith, Nat. Photonics **10**, 788 (2016).
6. M. R. Foreman, J. D. Swaim, and F. Vollmer, Adv. Opt. Photon. **7**, 168 (2015).
7. J. H. Wade and R. C. Bailey, Annu. Rev. Anal. Chem. **9**, 1 (2016).
8. R. Symes and J. P. Reid, Phys. Chem. Chem. Phys. **8**, 293 (2006).
9. C. R. Howle, C. J. Homer, R. J. Hopkins, and J. P. Reid, Phys. Chem. Chem. Phys. **9**, 5344 (2007).
10. T. Hümmer, J. Noe, M. S. Hofmann, T. W. Hänsch, and A. Högele, Nat. Commun. **7**, 12155 (2016).
11. K. Schaschek, J. Popp, and W. Kiefer, Ber. Bunsen. Phys. Chem. **97**, 1007 (1993).
12. J. Popp, M. Lankers, M. Trunk, I. Hartmann, E. Urlaub, and W. Kiefer, Appl. Spectrosc. **52**, 284 (1998).
13. J. Musick, J. Popp, M. Trunk, and W. Kiefer, Appl. Spectrosc. **52**, 692 (1998).
14. F. J. Timmermans, B. Liszka, A. T. M. Lenferink, H. A. G. M. van Wolferen, and C. Otto, J. Raman Spectrosc. **47**, 956 (2016).
15. I. Guerra and C. Cardell, J. Microsc. **260**, 47 (2015).
16. G. Wille, X. Bourrat, N. Maubec, and A. Lahfid, Micron **67**, 50 (2014).
17. H. W. P. Koops, J. Kretz, M. Rudolf, and M. Weber, J. Appl. Phys. **33**, 7099 (1994).
18. W. Ding, D. A. Dikin, X. Chen, R. D. Piner, R. S. Ruoff, E. Zussman, X. Wang, and X. Li, J. Appl. Phys. **98**, 014905 (2005).
19. S. Kim, D. D. Kulkarni, K. Rykaczewski, M. Henry, V. V. Tsukruk, and A. G. Fedorov, IEEE Trans. Nanotechnol. **11**, 1223 (2012).
20. J. S. Luo, C. S. Sung, W. S. Hsu, L. Y. Huang, and J. D. Russel, Microelectron. Reliab. **50**, 1446 (2010).
21. J. Lin, Y. Xu, Z. Fang, M. Wang, J. Song, N. Wang, L. Qiao, W. Fang, and Y. Cheng, Sci. Rep. **5**, 8072 (2015).
22. M. Amman, J. W. Sleight, D. R. Lombardi, R. E. Welser, M. R. Deshpande, M. A. Reed, and L. J. Guido, J. Vac. Sci. Technol. B **14**, 54 (1996).
23. A. C. Ferrari and J. Robertson, Phys. Rev. B **64**, 075414 (2001).
24. D. C. Joy and C. S. Joy, Micron **27**, 247 (1996).
25. S. Pang, R. E. Beckham, and K. E. Meissner, Appl. Phys. Lett. **92**, 221108 (2008).
26. F. Vollmer, D. Braun, and A. Libchaber, Appl. Phys. Lett. **80**, 4057 (2002).